Energy & Environmental Science

COMMUNICATION

View Article Online
View Journal | View Issue

Cite this: *Energy Environ. Sci.*, 2016, **9**, 2273

Received 9th March 2016,
Accepted 24th May 2016

DOI: 10.1039/c6ee00724d

www.rsc.org/ees

A high capacity thiospinel cathode for Mg batteries†

Xiaoqi Sun,[a] Patrick Bonnick,[a] Victor Duffort,[a] Miao Liu,[b] Ziqin Rong,[c] Kristin A. Persson,[b] Gerbrand Ceder[d] and Linda F. Nazar*[a]

Magnesium batteries are energy storage systems that potentially offer high energy density owing to their ability to employ magnesium metal as a negative electrode. Their development, however, has been thwarted by a paucity of functional positive electrode materials after the seminal discovery of the Mo_6S_8 Chevrel phase over 15 years ago. Herein, we report the second such material – a thiospinel – and demonstrate fully reversible Mg^{2+} electrochemical cycling *vs.* a Mg anode, which is complemented by diffraction and first principles calculations. The capacity approaches 80% of the theoretical value at a practical rate (C/5) at 60 °C, and yields a specific energy of 230 Wh kg^{-1}, twice that of the Chevrel benchmark. Our results emphasize the advantage in employing "soft" anions to achieve practical divalent cation mobility.

Although rechargeable batteries in commercial applications and academic research are currently dominated by lithium-ion batteries, considerable interest has arisen in cells which could employ a metallic negative electrode (anode), owing to their potentially greater energy density. Lithium batteries – that employ lithium metal – are one such example, but they are limited to special cases at present[1,2] owing to their propensity to form dendrites on cycling. Of the metals known to electrochemically deposit without dendrite formation, magnesium is of special interest.[3,4] In addition to its desirable electrochemical properties, including a volumetric energy density of 3833 mA h cm^{-3}, Mg metal offers good availability, low cost factors and safe handling in ambient atmosphere. This renders Mg rechargeable batteries compelling candidates for sustainable electrochemical storage devices at both large and intermediate scales. The first rechargeable Mg battery prototype reported in 2000 by Aurbach *et al.*[5] resulted from two major breakthroughs: the development of electrolytes based on the association of a Grignard species R–Mg–Cl with a strong Lewis acid such as $AlCl_3$[6,7] and the introduction of Chevrel phases, Mo_6Ch_8 with Ch = S, Se, as positive electrode materials coupled with a Mg anode.[8,9] Efforts to break past this pivotal discovery have proven challenging, however.

Magnesium electrochemistry is more difficult than that of its monovalent alkali cation cousins such as lithium and sodium. The lower mobility of Mg^{2+} ions within solid oxide hosts[10–14] and a probable higher energy penalty for the desolvation of Mg^{2+},[15] are among the limiting factors identified to date. As a result, the search for positive electrode materials able to reversibly intercalate Mg^{2+} and which present a higher energy density than Mo_6S_8 has been generally unrewarding and the Chevrel phase has remained the benchmark for magnesium batteries. To date, oxide cathode materials exhibit extremely sluggish kinetics,[16]

Broader context

With growing acceptance of the need to minimize fossil fuel consumption, the need for batteries with higher energy densities at much lower cost is intensifying. One of the promising new battery systems being studied at present is the magnesium battery. It relies on a Mg negative electrode, which does not grow dendrites during charging, and has twice the volumetric density of Li. Unfortunately, Mg battery development has been hindered by a lack of functional positive electrode materials since the seminal discovery of Mg insertion into the Chevrel phase (Mo_6S_8) in 2000. Herein, we report the second functional positive electrode material – the cubic thiospinel Ti_2S_4 – and explore the complexities of Mg-ion siting and mobility in the spinel lattice through X-ray diffraction and first principles calculations. Ti_2S_4 achieves 80% of its theoretical capacity at a rate of C/5 (discharge/charge in five hours) at 60 °C. Practically, this yields an energy density of 230 Wh kg^{-1}, which is twice that of the Chevrel phase benchmark under similar conditions. These findings highlight the importance of "soft" anions to achieve practical divalent cation mobility in the continuing search for positive electrode materials for the Mg battery.

[a] *Department of Chemistry and the Waterloo Institute of Nanotechnology, University of Waterloo, Waterloo, Ontario N2L 3G1, Canada. E-mail: lfnazar@uwaterloo.ca*
[b] *Applied Energy Materials Group, Lawrence Berkeley National Laboratory, CA 94720, USA*
[c] *Department of Materials Science and Engineering, Massachusetts Institute of Technology, Cambridge, MA 02139, USA*
[d] *Materials Science Division, Lawrence Berkeley National Laboratory, Berkeley, CA 94720, USA*

† Electronic supplementary information (ESI) available: Additional information pertaining to the method, and method validation are presented. See DOI: 10.1039/c6ee00724d

and conversion materials lack the required cycle life.[3] This led us to explore thiospinels, which benefit from a soft anion (*i.e.* sulphur) lattice. This leads to a weaker coulombic attraction between the guest Mg^{2+} and host sulphur lattice, which enhances ion mobility. Electrochemical Cu^{+} extraction from $CuTi_2S_4$ was reported long ago,[17] along with subsequent studies that demonstrated chemical magnesiation of the empty cubic thiospinel Ti_2S_4 lattice.[18–20] However, despite an initial tantalizing report,[21] reliable electrochemical cycling of Mg^{2+} in the Ti_2S_4 lattice has not been reported to date. An important computational study on magnesium mobility in layered TiS_2 and the thiospinel Ti_2S_4 suggested that these materials are unlikely to be suited for Mg (de)intercalation at room temperature owing to a migration barrier predicted to be about 800 meV.[22] However, even the Chevrel phase is difficult to fully recharge at room temperature[9] because ionic diffusion is thermally activated, and at room temperature half the Mg^{2+} is trapped in sites with higher migration barriers. One way to overcome the problem is to cycle at elevated temperature, as demonstrated for $Mg_xMo_6S_8$, where the performance of the material was greatly increased at 60 °C compared to room temperature.[23] This methodology is utilized here.

$CuTi_2S_4$ was prepared by literature methods[24] and Cu^{+} was extracted by oxidation.[25] Rietveld refinement[26] of the X-ray diffraction (XRD) patterns of the oxidized material (Fig. S1, ESI†), supported by EDX analysis, (Table S1, ESI†) indicates a single cubic *Fd*$\bar{3}$*m* phase with a stoichiometry of $Cu_{0.1}Ti_2S_4$ and a lattice parameter of 9.776 Å, indicating that some residual copper remains in the thiospinel. These results are in good agreement with Sinha *et al.*[27] and James *et al.*[28] where incomplete extraction of Cu^{+} suggests that band structure may play a role in determining the redox chemistry of Ti_2S_4. The Ti 3d band lies slightly above the S 3p band, which makes the former the main redox center.[29] However, during oxidation, the Ti 3d band drops closer to the S 3p band. It is possible that as the bands begin to overlap, some holes are produced in the S 3p band as proposed for other thiospinels where they are suggested to dominate. This makes further oxidation difficult due to the high electronegativity of sulphur.[30] This thiospinel material (labeled as cubic Ti_2S_4 or simply "C-Ti_2S_4" below) was used as the positive electrode in coin cells that employed Mg as the negative electrode and APC as the electrolyte.

Fig. 1 shows the resulting discharge and charge profiles of the cells comprised of C-Ti_2S_4 at different rates. Cells run in APC/THF (Fig. 1a) show that at C/20 (1C = 1 Mg^{2+}/C-Ti_2S_4, black curve), an initial discharge capacity of 200 mA h g^{-1} – corresponding to $Mg_{0.84}Ti_2S_4$ – was achieved with an overpotential of only 50 mV from equilibrium. The sloping curve between 1.5 V to 1 V demonstrates a solid-solution Mg^{2+} insertion mechanism, as previously predicted by theory.[22] As the cycling rates increased to C/10 and C/5, the discharge capacity dropped to 195 mA h g^{-1} and 190 mA h g^{-1}, respectively, demonstrating the surprisingly good rate capability of the material. At all three rates, the first charge shows minor irreversible capacity (10% at C/5), which disappears on the 2nd cycle (Fig. 1a inset). Long term cycling was examined in APC/tetraglyme (APC/G4), an electrolyte whose higher boiling point (275 °C) supports longer term cycling. Similar capacities of 195 mA h g^{-1} at C/20, dropping to 175 mA h g^{-1} at C/5, were observed (Fig. S2, ESI†). From cycle 2 onward (Fig. 1b), the drop levels off, and a capacity of 140 mA h g^{-1} is attained after 40 cycles at C/10. The origin of the cycling fade might be due to the micron-sized active material particles (Fig. S3, ESI†) that are large enough to kinetically trap Mg^{2+} during charge, which will be the subject of future studies. The present communication aims to report the overall new features and electrochemistry of cubic $Mg_xTi_2S_4$.

The reversible intercalation of Mg^{2+} into C-Ti_2S_4 was confirmed by X-ray diffraction (XRD) as shown in Fig. 2a, and by energy dispersive X-ray analysis (EDX, Table S1, ESI†). Rietveld[26] refinement of the discharged XRD pattern (Fig. 2b) indicated the preservation of the *Fd*$\bar{3}$*m* cubic spinel phase, with lattice parameters expanded to 10.097 Å from their pristine values (9.776 Å) on electrochemical magnesiation of 0.8 Mg. Fourier mapping carried out with Cu, Ti, and S occupying their normal sites revealed electron density on both the tetrahedral (8a) and octahedral (16c sites) (Fig. S4, ESI†). Mg was placed on both these sites in the subsequent refinements of Mg occupancy (see ESI† for details), resulting in ~30% occupation of the octahedral 16c site and ~20% on the tetrahedral 8a site (Table S2b, ESI†). The corresponding composition $Mg[oct]_{0.59(1)}Mg[tet]_{0.189(7)}Cu_{0.1}Ti_2S_4$ is in excellent agreement with the electrochemical capacity ($Mg_{0.84}Ti_2S_4$) and the EDX data (Table S1, ESI†). Only relatively minor shifts in the

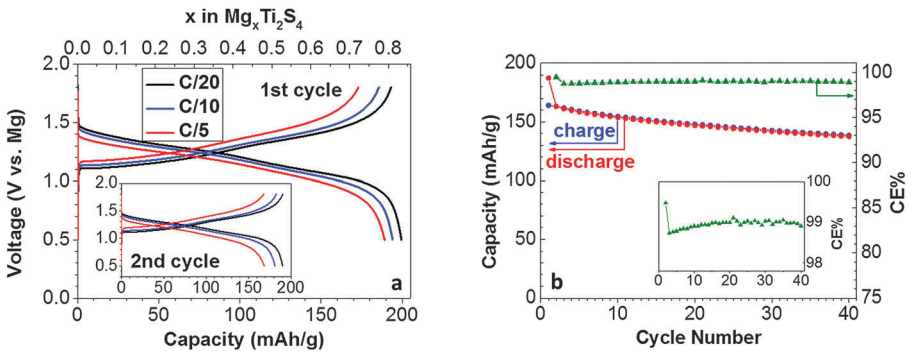

Fig. 1 Electrochemistry of C-Ti_2S_4 coin cells with an APC electrolyte and a Mg negative electrode at 60 °C. (a) Discharge and charge curves of the first and second (inset) cycles at various rates in APC/THF electrolyte. (b) Capacity and coulombic efficiency (CE) evolution at a C/10 rate in APC/G4 electrolyte (inset showing 99% CE).

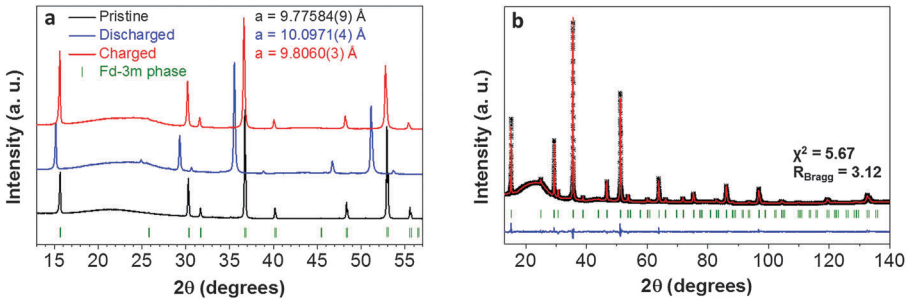

Fig. 2 XRD patterns of $Mg_xTi_2S_4$. (a) Comparison of the XRD pattern of the initial C-Ti_2S_4 spinel (black), with the discharged (blue) and charged (red) states. The electrodes were cycled in APC/THF electrolyte with a Mg anode at 60 °C and a C/20 rate. (b) Rietveld refinement fit of the discharged sample, $Mg_{0.8}Ti_2S_4$. Black crosses – experimental data, red lines – fitted data, blue line – difference curve between observed and calculated data, green ticks – the Bragg peak positions. The broad hump is a background signal from the X-ray capillary.

atomic positions occur on magnesiation (Table S2a and b, ESI†). Along with the moderate volume expansion on full insertion (10%), this confirms that the structure of the Ti_2S_4 thiospinel exhibits little distortion on Mg cycling, which promotes good capacity retention. Upon charging the material, the XRD pattern (red) reverts to the pristine composition with a cell parameter of a = 9.806 Å. EDX and XRD confirm that Mg^{2+} is essentially removed from the C-Ti_2S_4. The composition of $Mg_{0.08}Ti_2S_4$ determined by EDX (Table S1, ESI†) and the tiny increase in the lattice parameter (*vis a vis* 9.776 Å) are in accord with a trace of Mg remaining on the 16c site (Table S2c and Fig. S5, ESI†). Overall, the data unequivocally show that the electrochemical activity of the material is due to reversible (de)intercalation of Mg^{2+} into the spinel structure.

The above findings are consistent with our measurements of the self-diffusion coefficient of Mg^{2+} (D_{Mg}) using the galvanostatic intermittent titration technique (GITT)[31] at 60 °C (ESI†). The resulting D_{Mg} values, shown in Fig. 3a, were converted to activation energies (E_a) using the typical Arrhenius-type relation (see ESI†) and are shown in Fig. 3a as a function of state-of-discharge (x). First principles calculations of E_m in the thiospinel are shown in Fig. 3b at both the dilute (Ti_2S_4) and concentrated ($Mg_{7/8}Ti_2S_4$) limits. The barriers are lower than those reported in other work[22] due to the difference in lattice parameters used in the calculations; we used lattice parameters of 9.78 Å (the experimental value) for the dilute limit cubic Ti_2S_4, and 10.05 Å for the concentrated limit. The average calculated barrier height of about 550 meV agrees very well with the average experimentally determined E_a. In Fig. 3a, the increase in the barrier height to Mg^{2+} diffusion at $x > 0.6$ results in a kinetic limitation, explaining why we do not achieve $x = 1$ during discharge. Cycling $Mg_xTi_2S_4$ at 25 °C further slows down diffusion, which causes the potential to drop more quickly as shown in Fig. S6 (ESI†), yielding a capacity of about 130 mA h g^{-1}. At the end of discharge the experimental activation energy for Mg diffusion increases sharply. Calculations considering only a tri-vacancy diffusion mechanism[32] cannot explain this increase in E_a, as demonstrated by the lower diffusion barrier height in Fig. 3b at the concentrated limit. Instead, the reduced Mg^{2+} mobility near the end of discharge indicates the important role of site-disorder and/or Mg–Mg interaction in determining Mg^{2+} diffusivity. For example, at high Mg^{2+} concentration the number of possible tri-vacancy hops likely decreases, replaced by di-vacancy hops. A di-vacancy means that one of the three octahedral sites adjacent to the intermediate tetrahedral site is occupied, which increases the migration barrier. We find that the barrier for Mg^{2+} migration through the di-vacancy is about 200 meV higher than through the tri-vacancy, which will be detailed in subsequent reports.

Since Mg^{2+} occupation on the tetrahedral site was not identified in early studies of chemical magnesiation (albeit limited to $Mg_xTi_2S_4$ where $x < 0.5$[19]) we carried out first principles calculations to

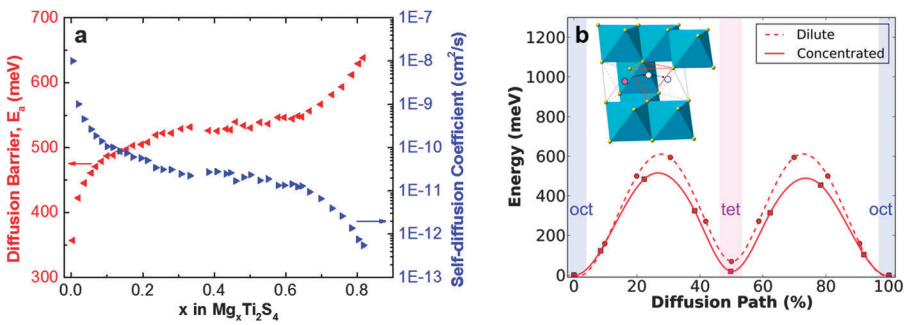

Fig. 3 (a) Mg self-diffusion coefficients and corresponding energy barriers of C-Ti_2S_4 determined by galvanostatic intermittent titration technique (GITT) at 60 °C; (b) energy barriers for Mg-ion migration in Ti_2S_4, calculated in the dilute and concentrated limits. Barriers are for migration through a tri-vacancy mechanism.

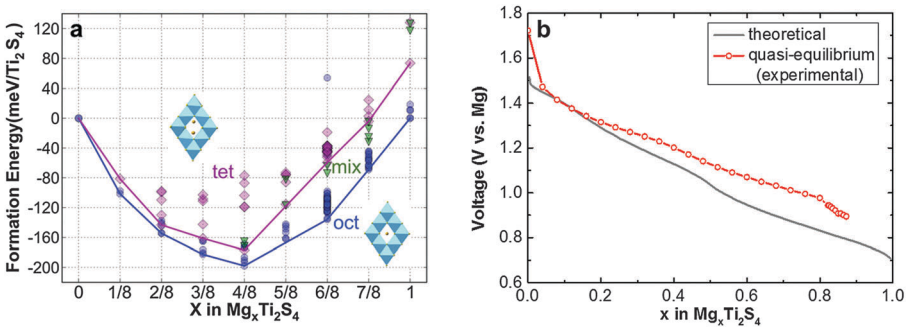

Fig. 4 (a) Calculated formation energies for different Mg occupancy orderings in Ti_2S_4 spinel. Three types of scenarios are considered: Mg occupying tetrahedral sites (magenta color, square markers), Mg occupying octahedral sites (blue color, round markers), and the co-existence of both tet. and oct. site-occupancies (green), (b) comparison of an experimental (grey) and theoretical (red) equilibrium voltage curve for $Mg_xTi_2S_4$. The theoretical curve was calculated by Emly *et al.* in ref. 22. The experimental curve was collected using a GITT experiment at 60 °C (see Methods, ESI†). The slight difference in the degree of the slope resulted from factors such as residual Cu in the structure, which was not included in the calculation.

explore the relative energy of compositions with various site occupations. Fig. 4a shows the formation energy of $Mg_xTi_2S_4$ configurations with Mg^{2+} cations in either tetrahedral sites (magenta squares), octahedral sites (blue circles), or mixed tetrahedral-octahedral (green triangles) configurations. While the lowest energy states clearly have Mg^{2+} in octahedral sites, the energy difference with tetrahedral and mixed occupancy states is rather small, making disorder across octahedral and tetrahedral sites likely. Note that because the energy in Fig. 4a is normalized per unit of Ti_2S_4, the increasing energy difference between structures with octahedral and tetrahedral occupancy with x is simply a reflection of the increased Mg^{2+} concentration in the structure, not necessarily of a change in site energy difference (see ESI† for details).

These findings shed light on the observed mixed site occupation at higher Mg content that we observed experimentally, with about 30% occupancy on octahedral sites (16c) and about 20% on tetrahedral sites (8a). A closer examination of partially discharged C-Ti_2S_4 materials (0.4 and 0.6 Mg/C-Ti_2S_4) reveals that Mg^{2+} only occupies octahedral sites (Tables S4 and S5, Fig. S7 and S8, ESI†) at this intercalation limit. Such preferential Mg^{2+} occupation on the octahedral site at low content was also observed by Bruce *et al.* in the entire range of their studies (0.07–0.5 Mg/Ti_2S_4).[19] A somewhat stepwise Mg^{2+} insertion behavior is therefore suggested by our findings, with the 16c site being filled first, followed by population of the 8a site that is driven by subtle thermodynamic and kinetic factors. The solid solution-like nature of the discharge/charge curves suggests that at the cross-over point, the energetics for occupation of either site are similar and the system lowers its (electrostatic) energy by distributing Mg^{2+} over both tetrahedral and octahedral sites. We propose that upon Mg^{2+} insertion beyond $x = 0.5$, energetics that result in coulombic repulsion favour redistribution amongst the possible sites. Based on our experimental results, this limitation occurs at about 0.6 Mg^{2+}/$Cu_{0.1}Ti_2S_4$. The Mg^{2+} diffusion pathways thus become partially hindered, which could be the reason behind the increase in E_a above about $x = 0.6$, explaining the deviation of our equilibrium electrochemical profile – obtained by the galvanostatic intermittent titration technique (GITT) – from that predicted for Mg occupation on the 16c octahedral site based on previously reported first principles calculations[22] (Fig. 4b). Thus, both thermodynamics (population of mixed oct-tet sites) and kinetics could, and probably do, contribute to the voltage drop at the end of discharge (Fig. S9, ESI†). Further detailed studies are underway in order to understand this complex behavior and its influence on the electrochemistry.

In summary, the thiospinel Ti_2S_4 shows promise as a new cathode material for Mg batteries, yielding a high capacity of 200 mA h g^{-1} at an average voltage of 1.2 V *vs.* Mg (corresponding to a volumetric energy density of about 350 Wh L^{-1} for a full Ti_2S_4–Mg cell). On subsequent cycles with a capacity of 150 mA h g^{-1}, the specific energy is 180 Wh kg^{-1}, almost twice that of the Chevrel phase at 100 Wh kg^{-1}. Despite the moderate Mg^{2+} diffusion barrier, spinel Ti_2S_4 exhibits excellent rate capabilities at 60 °C and the small volume change during cycling promotes good capacity retention. Subtle ordering of Mg^{2+} on the octahedral and tetrahedral sites of the thiospinel lattice at high Mg^{2+} concentrations results in complex behaviour that is the subject of our ongoing studies. As our understanding of this behaviour improves, so too should the cycle life. Approaches to improve the electrochemistry of Ti_2S_4 at room temperature, such as reducing particle sizes and using electrolytes with lower Mg^{2+} desolvation barriers, are under investigation. Given the rich chemistry of the thiospinel family, the discovery of facile, reversible Mg^{2+} intercalation in Ti_2S_4 provides an additional menu of options (apart from the Chevrel phase) which should accelerate the fundamental understanding of Mg^{2+} intercalation behavior in solid structures. This will directly contribute to the discovery of more Mg cathode candidates.

Acknowledgements

This work was supported by the Joint Center for Energy Storage Research (JCESR), an Energy Innovation Hub funded by the US Department of Energy (DOE), Office of Science, Basic Energy Sciences. NSERC is acknowledged by LFN for a Canada Research Chair.

Notes and references

1 M. B. Armand, J.-M. Chabagno and M. J. Duclot, *Poly-ethers as solid electrolytes in Fast Ion Transport in Solid Electrodes and Electrolytes*, Amsterdam, North-Holland, 1979.
2 L. Damen, J. Hassoun, M. Mastragostino and B. Scrosati, *J. Power Sources*, 2010, **195**, 6902–6904.
3 J. Muldoon, C. B. Bucur and T. Gregory, *Chem. Rev.*, 2014, **114**, 11683–11720.
4 H. D. Yoo, I. Shterenberg, Y. Gofer, G. Gershinsky, N. Pour and D. Aurbach, *Energy Environ. Sci.*, 2013, **6**, 2265–2279.
5 D. Aurbach, Z. Lu, A. Schechter, Y. Gofer, H. Gizbar, R. Turgeman, Y. Cohen, M. Moshkovich and E. Levi, *Nature*, 2000, **407**, 724–727.
6 D. Aurbach, H. Gizbar, H. Schechter, O. Chusid, E. E. Gottlieb, Y. Gofer and I. Goldberg, *J. Electrochem. Soc.*, 2002, **149**, A115–A121.
7 O. Mizrahi, N. Amir, E. Pollak, O. Chusid, V. Marks, H. Gottlieb, L. Larush, E. Zinigrad and D. Aurbach, *J. Electrochem. Soc.*, 2008, **155**, A103–A109.
8 E. Lancry, E. Levi, Y. Gofer, M. Levi, G. Salitra and D. Aurbach, *Chem. Mater.*, 2004, **16**, 2832–2838.
9 E. Levi, A. Mitelman, O. Isnard, M. Brunelli and D. Aurbach, *Inorg. Chem.*, 2008, **47**, 1975–1983.
10 G. G. Amatucci, F. Badway, A. Singhal, A. Singhal, B. Beaudoin, G. Skandan, T. Bowmer, I. Plitz, N. Pereira, T. Chapman and R. Jaworski, *J. Electrochem. Soc.*, 2001, **148**, A940–A950.
11 E. Levi, M. D. Levi, O. Chasid and D. Aurbach, *J. Electroceram.*, 2009, **22**, 13–19.
12 M. Liu, Z. Rong, R. Malik, P. Canepa, A. Jain, G. Ceder and K. A. Persson, *Energy Environ. Sci.*, 2015, **8**, 964–974.
13 G. S. Gautam, P. Canepa, R. Malik, M. Liu, K. A. Persson and G. Ceder, *Chem. Commun.*, 2015, **51**, 13619–13622.
14 S.-H. Bo, C. P. Grey and P. G. Khalifah, *Chem. Mater.*, 2015, **27**, 4630–4639.
15 L. F. Wan, B. R. Perdue, C. A. Apblett and D. Prendergast, *Chem. Mater.*, 2015, **27**, 5932–5940.
16 E. Levi, Y. Gofer and D. Aurbach, *Chem. Mater.*, 2010, **22**, 860–868.
17 R. Schöllhorn and A. Payer, *Angew. Chem., Int. Ed. Engl.*, 1985, **24**, 67–68.
18 P. G. Bruce, F. Krok, J. Nowinski, V. C. Gibson and K. Tavakkoli, *J. Mater. Chem.*, 1991, **1**, 705–706.
19 P. Lightfoot, F. Krok, J. L. Nowinski and P. G. Bruce, *J. Mater. Chem.*, 1992, **2**, 139–140.
20 P. G. Bruce, F. Krok, P. Lightfoot and J. L. Nowinski, *Solid State Ionics*, 1992, **53–56**, 351–355.
21 N. Amir, Y. Vestfrid, O. Chusid, Y. Gofer and D. Aurbach, *J. Power Sources*, 2007, **174**, 1234–1240.
22 A. Emly and A. Van der Ven, *Inorg. Chem.*, 2015, **54**, 4394–4402.
23 M. D. Levi, E. Lancry, H. Gizbar, Z. Lu, E. Levi, Y. Gofer and D. Aurbach, *J. Electrochem. Soc.*, 2004, **151**, A1044–A1051.
24 N. Soheilnia, K. M. Kleinke, E. Dashjav, H. L. Cuthbert, J. E. Greedan and H. Kleinke, *Inorg. Chem.*, 2004, **43**, 6473–6478.
25 P. G. Bruce and M. Y. Saidi, *J. Solid State Chem.*, 1990, **88**, 411–418.
26 H. M. Rietveld, *J. Appl. Crystallogr.*, 1969, **2**, 65–71.
27 S. Sinha and D. W. Murphy, *Solid State Ionics*, 1986, **20**, 81–84.
28 A. C. W. P. James, J. B. Goodenough and N. J. Clayden, *J. Solid State Chem.*, 1988, **77**, 356–365.
29 L. Benco, J.-L. Barras, M. Atanasov and C. Daul, *J. Solid State Chem.*, 1999, **145**, 503–510.
30 J. Rouxel and M. Tournoux, *Solid State Ionics*, 1996, **84**, 141–149.
31 W. Weppner and R. A. Huggins, *J. Electrochem. Soc.*, 1977, **124**, 1569–1578.
32 A. Van der Ven, J. Bhattacharya and A. A. Belak, *Acc. Chem. Res.*, 2013, **46**, 1216–1225.